

---

# Mixture Density Generative Adversarial Networks

---

Hamid Eghbal-zadeh <sup>†,\*</sup>, Werner Zellinger <sup>‡</sup>, Gerhard Widmer <sup>†</sup>

<sup>†</sup>: **Institute of Computational Perception**  
 Johannes Kepler University of Linz, Austria  
 {hamid.eghbal-zadeh,gerhard.widmer}@jku.at

<sup>‡</sup>: **Department of Knowledge-Based Mathematical Systems**  
 Johannes Kepler University of Linz, Austria  
 werner.zellinger@jku.at

## Abstract

Generative Adversarial Networks have surprising ability for generating sharp and realistic images, though they are known to suffer from the so-called *mode collapse problem*. In this paper, we propose a new GAN variant called Mixture Density GAN that while being capable of generating high-quality images, overcomes this problem by encouraging the Discriminator to form clusters in its embedding space, which in turn leads the Generator to exploit these and discover different modes in the data. This is achieved by positioning Gaussian density functions in the corners of a simplex, using the resulting Gaussian mixture as a likelihood function over discriminator embeddings, and formulating an objective function for GAN training that is based on these likelihoods. We show that the optimum of our training objective is attained if and only if the generated and the real distribution match exactly. We further support our theoretical results with empirical evaluations on one synthetic and several real image datasets (CIFAR-10, CelebA, MNIST, and Fashion-MNIST). We demonstrate empirically (1) the quality of the generated images in Mixture Density GAN and their strong similarity to real images, as measured by the Fréchet Inception Distance (FID), which compares very favourably with state-of-the-art methods, and (2) the ability to avoid mode collapse and discover all data modes.

## 1 Introduction

Generative Adversarial Networks (GANs) [12] learn an implicit estimate of the Probability Density Function (PDF) underlying a set of training data and can learn to generate realistic new samples. One of the known issues in GANs is the so-called *mode collapse* [1, 11, 23], where the generator memorizes a few training examples and all the generated examples are similar to only those. These memorized examples are known as *modes*. Although for the generator having a few – but good – modes for generated images is enough to fool the discriminator, the result is not a good generative model: when mode collapse happens, the generator is only capable of generating examples close to these modes and fails to generate a high variety from different prototypes available in the training data.

In this paper, we propose *Mixture Density GAN* that is capable of generating high-quality samples, and in addition copes with mode collapse problem and enables the GAN to generate samples with a

---

\*This work was supported by the Austrian Ministry for Transport, Innovation & Technology, the Ministry of Science, Research & Economy, and the Province of Upper Austria in the frame of the COMET center SCCH.

high variety. The central idea of **Mixture Density GAN (MD-GAN)** is to enable the discriminator to create several clusters in its output embedding space for real images, and therefore provides better means to distinguish not only real and fake, but also between different kinds of real images.

The discriminator in MD-GAN forms a number of clusters<sup>2</sup> with embeddings of real images which represent clusters in the real data. To fool the discriminator, the generator then has to generate images that discriminator has to embed close to the center of these clusters. As there are multiple clusters, the generator can discover various modes by generating images that end up in various clusters.

MD-GAN’s Discriminator uses a  $d$ -dimensional embedding space and is provided with an objective function that pushes it towards forming clusters in this space which are arranged in the form of a *Simplex*<sup>3</sup>: each cluster center is located in one of the vertices of this simplex. In our empirical experiments, we use four benchmark datasets of images and one synthetic dataset to demonstrate the ability of MD-GAN to generate samples with good quality and high variety, and to avoid mode collapse. Comparing our results to state-of-the-art methods in terms of the Fréchet Inception Distance (FID) [14] as well as the number of discovered modes with high-quality generated examples [27], we will demonstrate that MD-GAN can achieve state-of-the-art level results. Further, we will show that MD-GAN achieves better FIDs, also can discover more modes with more high-quality generated samples, on all the datasets, compared to all the baselines.

## 2 Related Work

GANs exhibit a surprising ability to generate sharp and realistic images – in contrast to the blurry images generated via other techniques such as VAEs [15] –, they are known to be difficult to train.

Since the advent of the first GAN (vanilla) [12], many variations have been proposed to make training easier by optimizing an alternative objective function. The Energy-Based GAN (EBGAN) [33] and its improved variant Boundary-Equilibrium GAN (BEGAN) [4] use an auto-encoder as discriminator and reconstruction loss as an energy function that assigns low energies to the regions near the data manifold and higher energies to others. The Wasserstein GAN (WGAN) [2] and Wasserstein GAN with Gradient Penalty (WGAN-GP) [13] minimize the Wasserstein distance between the activations of real and fake images in a Lipschitz-constraint discriminator.

Some authors have investigated solutions to the *mode collapse* problem. The Bayesian GAN [26] uses a Bayesian formulation and optimizes a GAN using stochastic gradient Hamiltonian Monte Carlo, which makes for more diverse generated samples. Bayesian GAN requires Monte Carlo (MC) sampling to marginalize the weights of the generator and discriminator networks and therefore, can be computationally expensive. While the Bayesian GAN can generate a high variety of samples, it does not demonstrate the ability to generate sharp and realistic images with high quality. Multi-discriminator GAN [9] uses multiple discriminators to overcome the mode collapse. Although it improves the mode-discovery, it is computationally expensive as one has to train multiple discriminators in each epoch. Coulomb GAN [29] poses the GAN learning problem as a potential field of charged particles, where generated samples are attracted to training set samples but repel each other. Its discriminator needs to be updated twice: once to generate the mini-batch-specific potential, and a second time for the evaluation of the potential and its approximation. Therefore it requires extra computation. VEEGAN [27], uses a discriminator that auto-encodes Gaussian noise and succeeds in discovering the modes in the data, though it does not assess the quality of generated images.

Our work is different than [9] since we only use a single discriminator in contrast with the multi-discriminator GAN which uses an ensemble of discriminators, and also differs from Coulomb GAN [29] as it requires two-times updates of the discriminator. Hence, MD-GAN is computationally more efficient and memory-friendly. Also, MD-GAN differs from VEEGAN [27] as we do not auto-encode the noise. This might be problematic as VEEGAN’s objective is built upon Gaussian distribution used in both discriminator and the generator which has to match. Hence it limits VEEGAN since choosing the distribution of the noise in the generator can indeed negatively effect the quality and diversity of a GAN as discussed in [30]. In contrast, MD-GAN allows the noise

---

<sup>2</sup>The number of clusters is a parameter that can be set.

<sup>3</sup>A simplex is defined as a generalization of the notion of a tetrahedron with  $d$  dimensions and  $d + 1$  vertices[25].

distribution in the generator to be selected independently from the embedding distribution of the discriminator.

### 3 Mixture Density Generative Adversarial Networks

In this section, we explain the intuition, the objectives and the training procedure in MD-GAN. But before doing so, we quickly recall the vanilla GAN and its objectives.

#### 3.1 Generative Adversarial Networks

A GAN usually consists of two neural networks competing with each other: (1) A generator network  $G$  that decodes noise vectors into images, and (2) a discriminator network  $D$  that encodes images into a notion of probability of an image being real or fake. A *real* image is one from a dataset of training images; an image generated by the generator is considered a *'fake'*.

The generator tries to fool the discriminator by learning to generate images that in the discriminator produce high probabilities of being real and that thus cannot be distinguished from real images by the discriminator. For this game to go on, the discriminator is trained to produce high probabilities for images coming from the real image dataset, and low probabilities for images coming from the generator. As training continues, the generator learns to generate images that produce high probabilities in the discriminator, which usually look also realistic for humans and are visually similar to samples from the training dataset.

#### 3.2 The Vanilla GAN Objectives

The loss of the discriminator  $D$  of the Vanilla GAN shall be maximized and was defined and introduced in [12] as

$$\mathcal{L}(D) = \mathbb{E}_{\mathbf{x} \sim p_{data}} [\log D(\mathbf{x})] + \mathbb{E}_{\mathbf{z} \sim p_z} [\log(1 - D(G(\mathbf{z})))] \quad (1)$$

where for a given input image  $\mathbf{x}$ , the discriminator  $D$  outputs an estimated probability of the image coming from the dataset of real images.  $p_{data}$  represents the distribution of real images, and  $p_z$  represents the distribution of noise. For the generator, two objectives are provided: a *Minimax objective* with theoretical results regarding global optimum, and a *Non-Saturating heuristic objective* that is used in most experiments and leads to more stable training and better empirical results. The objective for the generator  $G$  and its alternative (both to be minimized) are:

$$\mathbf{Minimax} : \mathcal{L}(G) = \mathbb{E}_{\mathbf{z} \sim p_z} [\log D(1 - G(\mathbf{z}))] \quad (2a)$$

$$\mathbf{Non-saturating} : \mathcal{L}(G) = -\mathbb{E}_{\mathbf{z} \sim p_z} [\log D(G(\mathbf{z}))] \quad (2b)$$

where  $\mathbf{z}$  is an observation from a random distribution  $p_z$ ; generator  $G$  creates a fake image using this  $\mathbf{z}$ . These two objectives and their differences are discussed in detail in [11, 10]. In the present paper, vanilla GAN is used to refer to this GAN [12] with Non-Saturating Loss.

#### 3.3 Mixture Density GAN: The Intuition

As explained in the introduction, the basic idea in Mixture Density GAN is to encourage the discriminator to form a number of clusters from embeddings of real images. As also mentioned above, these clusters will be positioned in an equi-distant way, their center vectors forming a *simplex*. Each cluster is represented by a Gaussian kernel, the whole collection thus makes up a *mixture of Gaussians*, which we will call a *Simplex Gaussian Mixture Model (SGMM)*. Each of the clusters draw embeddings of fake images towards their center. This is achieved by using the SGMM as a likelihood function. Each Gaussian kernel spreads its density over the embedding space: the closer an embedding to the center of a cluster, the more density it gets and therefore, the more likelihood reward it receives.

By defining a likelihood function with the parameters of a SGMM, in each update we train the discriminator to encode real images to the centers of the clusters. The resulting SGMM creates a mixture of clusters that draws the real embeddings towards the cluster centers (see Figure 1). Because of the multiple clusters, the generator will be rewarded if it generates samples that end up in any of these clusters. Thus, if the fake embeddings are well spread around the clusters – which they are

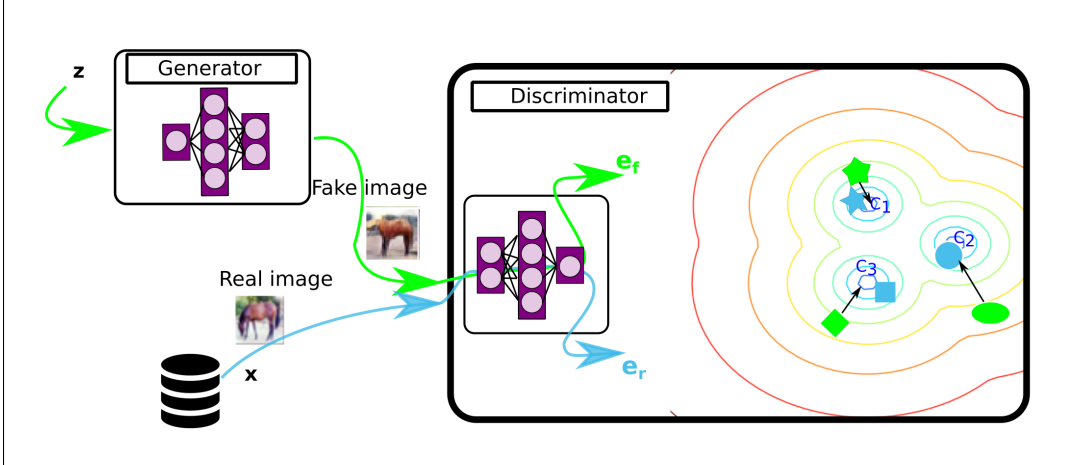


Figure 1: Block diagram of Mixture Density GAN. This figure should be viewed in colour.

likely to be at the beginning of training, when they are essentially just random projections –, it is likely that most of the clusters will draw the fake embeddings. Therefore, the generator will tend to learn to generate samples with more variety to cover all of the clusters, which ideally results in discovering the modes present in the data and directly addresses the mode collapse problem. On the other hand, it is reasonable to expect the discriminator to create such clusters based on relevant similarities in the data, since it is trained as a classifier and therefore needs to learn a meaningful distance in its embedding space. Experiments described in results Section will confirm our intuition.

### 3.4 Mixture Density GAN: The Model

As in the vanilla GAN, MD-GAN consists of a generator  $G$  and a discriminator  $D$ . MD-GAN uses a mixture of Gaussians in its objective functions whose mean vectors are placed in the cartesian coordinates of the vertices in a  $d$ -dimensional simplex.

**Discriminator:** The discriminator  $D$  in MD-GAN is a neural network with  $d$ -dimensional output. For an input image  $x$ , the discriminator creates an embedding  $e$  which is simply the activations of the last layer of the network for input  $x$ .

The SGMM in MD-GAN is a Gaussian mixture with the following properties:

1. The individual components are  $d$ -dimensional multivariate Gaussians (where  $d$  is the output/embedding dimensionality of the discriminator network).
2. The model comprises  $d + 1$  Gaussian components, whose mean vectors are exactly the coordinates of the vertices of a simplex.
3. The covariance matrices are diagonal and have equal values on the main diagonal, in all the components. Thus, all components are spherical Gaussians.
4. The component weights  $w_i$  are either 1 if the component produces the highest likelihood among all components, or 0 otherwise.

For an embedding  $e$  produced by the discriminator  $D$ , we define the following *likelihood function*:

$$lk(e) = \sum_{i=1}^n w_i \cdot \Phi(e; \mu_i, \Sigma_i) \quad (3)$$

where  $\Phi$  is the Gaussian PDF,  $w_i$  is the mixture weight,  $\mu_i$  is the mean vector, and  $\Sigma_i$  is the covariance matrix for Gaussian component  $i$ .

When a discrimination between real and fake images is needed, the discriminator first encodes the input image  $x$  into the embedding  $e$ . Then, a likelihood  $lk(e)$  is calculated for this embedding.  $lk(e)$

will be interpreted as the probability of  $e$  being an embedding of a real image, given the current model.

**Generator:** The generator  $G$  in MD-GAN is a regular neural network decoder, decoding a random noise  $z$  from a random distribution  $P_z$  into an image.

### 3.5 The Mixture Density GAN Objectives

Denoting the encoding (output of the encoder, also referred to as the embedding) of an image  $\mathbf{x}$  by discriminator  $D$  as  $D(\mathbf{x})$ , we propose the MD-GAN’s objectives as follows:

$$\begin{aligned} \min_G \max_D \mathcal{L}(G, D) = \\ \min_G \max_D \mathbb{E}_{\mathbf{x} \sim p_{data}} [\log(\text{lk}(D(\mathbf{x})))] \\ + \mathbb{E}_{\mathbf{z} \sim p_z} [\log(\lambda - \text{lk}(D(G(\mathbf{z}))))] \end{aligned} \quad (4)$$

where the likelihood  $\text{lk}(e)$  for the given image embedding  $e = D(\mathbf{x})$  is as defined in Eq.(3). We set  $\lambda$  to be the maximum value of the likelihood function  $\text{lk}$  in order to have only positive values in the logarithm in Eq.(4) (see also Experimental Setup Section.)

### 3.6 Likelihood Assignment

The likelihoods of the embeddings are assigned in the following way:

1. Likelihoods of the embedding of a *real image* are computed separately for each of the Gaussian components.
2. To calculate the final likelihood assigned to an embedding of a *real image*, only the likelihood of the component which produced the highest value is used.
3. Similar to real images, likelihood computation for *fake images* are calculated by assigning the density value of the component that gives the highest value for  $e$ .

As discussed in [5], a Gaussian mixture can have more high-probability picks than its components<sup>4</sup> if the mean of the components are close to each other and the variance is relatively high. If the variance of the components are large enough, these extra high-probability areas can be dominating and therefore problematic for likelihood assignment. To avoid such issues, we use a small-enough variance (based on the guidelines provided in [6] around 20%-30% of the distance between the components).

## 4 Theoretical Discussion

Recall that our goal is to allow multiple data clusters in the discriminator’s embedding space while preserving the discriminative power of the generative adversarial model proposed in [12]:

**Proposition 1 (Goodfellow et al. 2014)** For  $G$  fixed and  $\mathcal{L}(D)$  being the discriminator loss as described in Eq.(1), the optimum discriminator<sup>5</sup>  $D_G^* := \arg \max_D \mathcal{L}(D)$  is given by

$$D_G^*(\mathbf{x}) = \frac{p_{data}(\mathbf{x})}{p_{data}(\mathbf{x}) + p_{gen}(\mathbf{x})}.$$

Let  $\lambda$  be the maximum of the likelihood function and  $p_{gen}$  represents the distribution of generated images. We define a new discriminator function  $\tilde{D}$  by putting  $\tilde{D}(\mathbf{x}) := \text{lk}(D(\mathbf{x}))/\lambda$  which normalizes the likelihood function and yields output values in the unit interval. By applying Proposition 1 we obtain that

$$\text{lk}(D^*(\mathbf{x})) = \lambda \cdot \frac{p_{data}(\mathbf{x})}{p_{data}(\mathbf{x}) + p_{gen}(\mathbf{x})}, \quad (5)$$

<sup>4</sup><http://www.cs.toronto.edu/~miguel/research/GMmodes.html>

<sup>5</sup>We keep the notation consistent with [12, Proposition 1]

for an optimum  $D^* := \arg \max_D \mathcal{L}(G, D)$  of the MD-GAN objective function in Eq.(4) with fixed  $G$ . Eq.(5) characterizes the multiple solutions of the discriminator objective. In the case of  $\lambda = 1$  and  $lk$  being the identity function, the discriminator solution of [12] is obtained, where the value of  $D^*(x)$  is one if and only if  $p_{\text{gen}}(x) = 0$ . In contrast, in our case,  $p_{\text{gen}}(x) = 0$  allows  $D^*(x)$  to be such that the Gaussian likelihood is maximized. Thus, Eq.(5) directly implements our idea of splitting up the optimal solutions to create more meaningful clusters in the embedding space.

For example, let us consider the one-dimensional case with the likelihood function defined by

$$lk(e) := \frac{1}{2}\Phi(e; -1, \frac{1}{4}) + \frac{1}{2}\Phi(e; 1, \frac{1}{4})$$

Then, for a point  $x_0$  with  $p_{\text{gen}}(x_0) = 0$ , Eq.(5) reduces to  $lk(D^*(x_0)) = \lambda$ . This implies that the optimal discriminator  $D^*$  fulfills either  $D^*(x_0) \simeq 1$  or  $D^*(x_0) \simeq -1$ , which, for suitable covariance of the likelihood function, are near the means of the component Gaussian densities. For  $x_0$  with  $p_{\text{gen}}(x_0) \neq 0$  four different global optimal solutions for  $D(x_0)$  exist.

The following Theorem 1 follows from [12, Theorem 1] and it shows that the optimum of our approach is achieved if and only if the distribution of the real images and the distribution of the generated images match exactly.

**Theorem 1** *Under the assumption of an optimal discriminator  $D^*$  as characterized by Eq.(5), the global optimum of the training criterion  $\min_G \mathcal{L}(G, D^*)$  in Eq.(4) is achieved if and only if  $p_{\text{data}} = p_{\text{gen}}$ .*

#### 4.0.1 Proof of Theorem 1

Under the assumption of an optimal discriminator  $D^*$ , characterized by Eq.(5), our objective  $\min_G \mathcal{L}(G, D^*)$  can be reformulated as

$$\begin{aligned} \min_G \mathcal{L}(G, D^*) &= \min_G \mathbb{E}_{\mathbf{x} \sim p_{\text{data}}} \left[ \log \left( \lambda \cdot \frac{p_{\text{data}}(\mathbf{x})}{p_{\text{data}}(\mathbf{x}) + p_{\text{gen}}(\mathbf{x})} \right) \right] \\ &+ \mathbb{E}_{\mathbf{x} \sim p_{\text{gen}}} \left[ \log \left( \lambda - \lambda \cdot \frac{p_{\text{data}}(\mathbf{x})}{p_{\text{data}}(\mathbf{x}) + p_{\text{gen}}(\mathbf{x})} \right) \right] \\ &= 2 \log(\lambda) \\ &+ \min_G \mathbb{E}_{\mathbf{x} \sim p_{\text{data}}} \left[ \log \left( \frac{p_{\text{data}}(\mathbf{x})}{p_{\text{data}}(\mathbf{x}) + p_{\text{gen}}(\mathbf{x})} \right) \right] \\ &+ \mathbb{E}_{\mathbf{x} \sim p_{\text{gen}}} \left[ \log \left( \frac{p_{\text{gen}}(\mathbf{x})}{p_{\text{data}}(\mathbf{x}) + p_{\text{gen}}(\mathbf{x})} \right) \right]. \end{aligned}$$

The optimality of our approach then follows from Theorem 1 in [12]. ■

## 5 Empirical Results

### 5.1 Evaluation Method

In our empirical results, we focus on two aspects: (1) the quality of the generated images, and (2) the power of MD-GAN in dealing with mode collapse and discovering all data clusters.

#### 5.1.1 Quality assessment

For the quality assessment in real images, we follow the procedure in [22] which carried out a large-scale study on many of the GAN variants and reported performance measures on four benchmark datasets. As the state-of-the-art measure, we use the *Fréchet Inception Distance* [14] to evaluate

the quality of the generated images in GANs. FID measures the distance between two Gaussians created by embeddings of real and fake images. These embeddings are created using an *Inception Network* [28] trained on the ImageNet dataset [18]. The FID is defined as follows:

$$FID(e_r, e_f) = \|\mu_{e_r} - \mu_{e_f}\|_2^2 + \text{Tr}(\Sigma_{e_r} + \Sigma_{e_f} - 2(\Sigma_{e_r}\Sigma_{e_f})^{\frac{1}{2}}) \quad (6)$$

where  $(\mu_{e_r}, \Sigma_{e_r})$  are first and second momentum of embeddings of a set of real images, and  $(\mu_{e_f}, \Sigma_{e_f})$  are first and second momentum of embeddings of fake images generated by a GAN. These embeddings are taken from the trained inception network. The FID results are computed using the provided code and trained inception model from the github repository<sup>6</sup> of the main author of the FID paper [14].

Since we use results from [22] as our baselines on 4 real image datasets, we also follow their FID computation procedure which includes 10k sampling of real and 10k sampling of generated images.

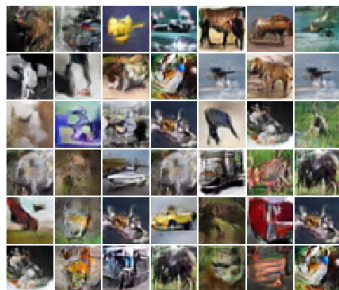
We use four popular image benchmark datasets for evaluation generative models: namely MNIST(28 × 28 gray-scale) [19], Fashion-MNIST(28 × 28 gray-scale) [32], CIFAR-10(32 × 32 RGB) [17] and CelebA(64 × 64 RGB) [21]. For a fair comparison, we use the same DCGAN architectures, hyper-parameters, optimisation and training epochs as in [22].



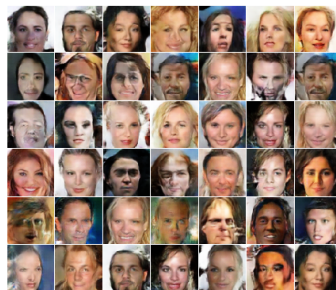
(a) MNIST.



(b) Fashion-MNIST.



(c) CIFAR-10.



(d) CelebA.

Figure 2: Randomly chosen generated examples of MD-GAN.

### 5.1.2 Mode-collapse

For mode-collapse experiments, we use an evaluation used in [29, 20, 27] for comparing the coping ability of different GAN variants with mode collapse. We use the same synthetic dataset as used in [29, 20, 27] with pre-defined clusters in a 2D input space. We use the evaluation measure proposed in [27] and report the number of discovered clusters and the quality of the generated examples in terms of their distance from the mean of each cluster. A generated data is considered high-quality if it is within less than  $3 \times std$  of the mean of a cluster. We use the same network architectures, hyper-parameters, optimisation and training epochs as in [27].

<sup>6</sup><https://github.com/bioinf-jku/TTUR>

## 5.2 Experimental Setup

### 5.2.1 Numerical computation of $\lambda$

: We compute the maximum value of the likelihood function using gradient descent. This is achieved by minimizing  $-\log(\text{lk}(D(\mathbf{x})))$  as defined in eq.(4) where  $D(\mathbf{x})$  is a feed-forward neural network with only one dense layer and trained on a single and fixed data point. The likelihood value of the data point then converges to the necessary maximum [5].

### 5.2.2 Network architectures

: The architectures used in our experiments are the same as used in [26] for synthetic data and in [22] for image experiments. The last layer in the discriminator of MD-GAN has the dimensionality of our simplex. The precise network architectures used can be found in Appendix as well as in the code in our github repository<sup>7</sup>.

### 5.2.3 Hyper-parameters and reproducibility

: We provide empirical results using two different number of clusters (8 and 10) and two different variances to demonstrate the effect of our hyper-parameters.

Having a look at the class distribution of the datasets used, we can see that there are 10 classes in CIFAR-10, MNIST and Fashion-MNIST; CelebA has 40 binary attributes and 25 Gaussians are used to generate our synthetic dataset. Therefore we believe the choices of number of clusters in MD-GAN for the reported results are in a reasonable range and close to those in the used datasets. In addition, since we would like to have a consistent hyper-parameterisation across all experiments, we report the results using two cluster numbers in all experiments.

Additionally, we provide the results for the variance of 0.25/0.25 and 0.28/0.25 (variance for real / variance for fake) for pairs in our likelihood function to demonstrate the effect of the variance. We already justified this choice as discussed in the Likelihood assignment Section. We specifically choose the latter combination to demonstrate that it is possible to choose different variances for real and fake.

Although we use very different datasets with different characteristics, we keep these hyper-parameters the same in all our experiments to demonstrate their effects. The vertices of our simplex have a distance of one from one another. The variances in the diagonal of the covariance matrices in all experiments with real images are set to 0.25 and 0.28 as discussed above.

We use the noise distributions and dimensionality, learning rates, batch sizes and optimization reported in [22] for all experiments on real images and those reported in [27] for mode collapsing experiments.

Our experiments are implemented in Python using Theano library [3] for automatic differentiation and Lasagne library [7] for neural network layers and optimization. To ensure reproducibility of our experimental results, the source code of our experiments is available online.<sup>8</sup>

## 5.3 Results

**Analysis of Mode Collapse Behavior:** We provide two sets of results on mode collapse: 1) visualizing the discovered clusters using different GANs, and 2) We report the number of discovered modes and high-quality generated data<sup>9</sup> as proposed in [27] on a synthetic dataset. The synthetic data consists of 100K 2D data points generated from a mixture of 25 Gaussians, This dataset was used in [20, 8] to study mode collapse behaviors in GANs. An example of data sampled from these Gaussians is shown in Figure 3a. Figure 3 shows our first mode collapse experimental results on this data set.

As can be seen, WGAN (Fig. 3c) exhibits a strong mode-collapsing behavior and fails to discover many of the Gaussian centers and overall, cannot produce a distribution similar to the real data distribution. Vanilla GAN (Fig. 3d) discovers most of the modes, but misses some of them. MD-GAN

<sup>7</sup>The repository will be added to the camera-ready version

<sup>8</sup>The source code will be uploaded to github, and the link will be provided in the camera-ready version.

<sup>9</sup>Data points with less than  $3 \times \text{std}$  distance from the mean of a cluster are considered high-quality.



(Fig. 3b) as well as Geometric GAN (GGAN in Fig. 3e) avoids mode collapsing and successfully discover all the modes and generate data that exhibits a distribution similar to the real data.

Figures 3f to 3j show the evolution of generated samples in MD-GAN. As can be seen, the data generated in early epochs is uniformly spread out over data space. As MD-GAN keeps training, a pattern becomes visible. The network discovers the overall distribution of the data and first moves the data points into four square-like areas (Fig. 3h) and further forms lines that connect the modes (Figure 3i). As training continues, the clusters disconnect and further concentrate, which in the end results in a distribution very similar to the real data (Figure 3j).

We also have visualized the *embeddings* of the discriminator for real data, by projecting them into 2D via PCA [31]. The plots can be found in Figures 3k-3o. Embeddings of data points coming from the same Gaussian in the training data have been given the same colour. It is quite apparent that clusters of different colours emerge in the discriminator’s embedding space when real data is used. As we expected, these clusters reflect similarities/distances in input data space: as the discriminator further differentiates the data into more specific clusters (Fig. 3o), we see that data points from the same cluster (colour) in the input data tend to be embedded in coherent clusters.

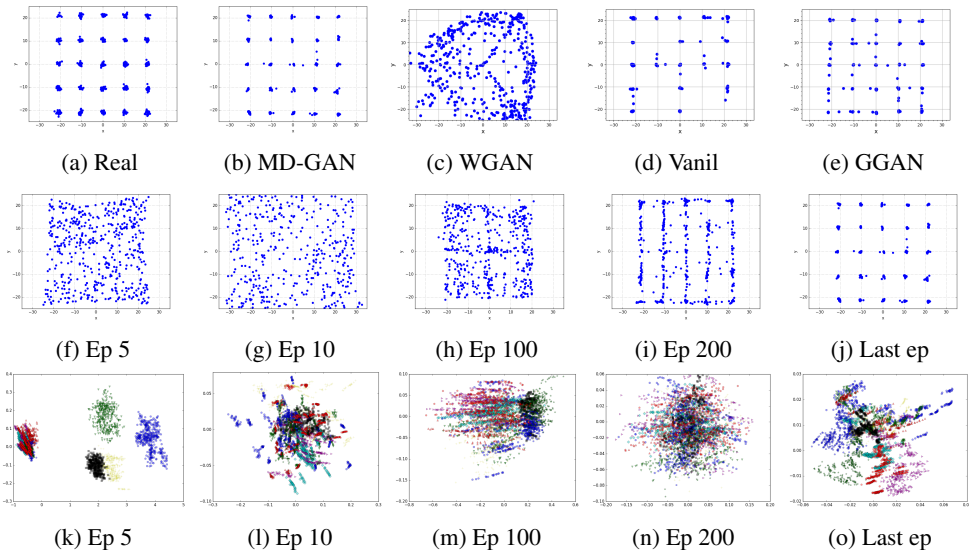


Figure 3: a-e) Examples generated on our synthetic dataset via different methods. Results of c-d are taken from[20]. f-j) Samples generated by Mixture Density GAN’s generator in different epochs. k-o) 2D PCA-projected embeddings of Mixture Density GAN’s discriminator for real data in different epochs. Embeddings of data points coming from the same input Gaussian have the same colour. Vanilla:[12],Wasserstein:[2],GGAN:[20]

Our second mode collapse experiments are provided in Table 1. As can be seen, MD-GAN discovers all the modes and at the same time, manages to generate significantly more high-quality data points compared to all the baselines.

**Real Image Data and Quality of Generated Images:** The quantitative results of our experiments with the four real image data sets are summarized in Table 2, where we compare the FIDs achieved by MD-GAN with the results of other GAN variants reported in [22].

#### 5.4 Discussions

As can be seen in the mode collapse experiments in the results Section, MD-GAN manages to discover all the modes in the data and significantly outperforms all the baselines. Comparing different hyper-parameterisations show that using less components results in generating more high-quality examples. Also the differences in variance does not seem to be very crucial compared to the number of components.

Table 1: Results of mode collapse experiments. Number of the captured modes as well as percentage of high-quality generated examples with less than 3 std from the mean of each mode. All the results are the average of 5 runs.

\*) The results are taken from[27].

**C**: # of components. **varR**: variance used for real. **varF**: variance used for fake.

method \ measure	# of modes (max 25)	% hq ( $\leq 3 \times std$ )		
Vanilla* [12]	3.3	0.5		
ALI* [8]	15.8	1.6		
Unrolled GAN* [24]	23.6	16		
VEEGAN* [27]	24.6	40		
WGAN-GP [13]	24	12.69		
<b>MD-GAN**</b>				
<b>C</b>	<b>varR</b>	<b>varF</b>		
8	0.25	0.25	<b>25</b>	<b>79.36</b>
8	0.28	0.25	<b>25</b>	<b>77.48</b>
10	0.25	0.25	<b>25</b>	<b>59.56</b>
10	0.28	0.25	<b>25</b>	<b>68.48</b>

Table 2: FIDs on different datasets from different methods. \*) Results from[22] which are best FIDs obtained in a large-scale hyper-parameter search for each data set. Lower FID values represent higher quality for generated images.

**C**: # of components. **varR**: variance used for real. **varF**: variance used for fake.

method \ db	MNIST	:Fashion-MNIST	Cifar10	CelebA		
Real images*	1.2	2.6	5.1	2.2		
Vanilla* [12]	6.7	26.6	58.6	58.0		
WGAN* [2]	6.8	18.0	55.9	42.9		
WGAN-GP* [13]	8.9	20.6	52.9	26.8		
DRAGAN* [16]	7.7	26.0	68.5	41.4		
BEGAN* [4]	12.3	33.2	71.4	38.1		
<b>MD-GAN</b>						
<b>C</b>	<b>varR</b>	<b>varF</b>				
8	0.25	0.25	5.98	<b>10.47</b>	41.47	31.86
8	0.28	0.25	6.29	11.79	<b>36.80</b>	<b>24.51</b>
10	0.25	0.25	5.59	13.74	47.96	31.55
10	0.28	0.25	<b>4.97</b>	13.03	38.84	28.44

For the results on real images, it can be seen that MD-GAN is capable of generating state-of-the-art results in term of FID in all datasets. In fact, MD-GAN achieves the lowest FID (lower is better) among all baselines. Analysing different hyper-parameterisations show that in FID, using slightly higher variance for real embeddings performs better in most of the cases in contrast with mode collapsing experiments. And our results suggests that although both 8 and 10 components performed better than all the baselines, the lower number of components performed slightly better in contrast with mode collapsing results.

These observations suggest that using slightly less number of clusters than the number of available classes is suitable. In addition, it seems that using slightly larger variance for reals than fakes in the likelihood improves the overall quality of the generated samples. This latter can be explained as the variance for real images increases, the discriminator can be trained easier and hence better embeddings can be formed that represent the data clusters, while keeping the variance small for fake embeddings prevents the low-quality images from receiving high likelihoods.

## 6 Conclusion

In this paper, we proposed a novel GAN variant called Mixture Density GAN, which succeeds in generating high-quality images and in addition alleviates the mode collapse problem by allowing the Discriminator to form separable clusters in its embedding space, which in turn leads the Generator to generate data with more variety. We analysed the optimum discriminator and showed that it is achieved when the generated and the real distribution match exactly and further discussed the relations to the vanilla GAN. We demonstrated the ability of Mixture Density GAN to deal with mode collapse and generate realistic images using a synthetic dataset and 4 image benchmarks. We further reported objective evaluation results using FID and mode collapse evaluation measures demonstrated that Mixture Density GAN achieved the best results of all compared baselines on all datasets, in terms of FID and the number of discovered modes with high-quality generated data.

## References

- [1] Martin Arjovsky and Léon Bottou. Towards principled methods for training generative adversarial networks. In *NIPS 2016 Workshop on Adversarial Training. In review for ICLR*, volume 2016, 2017.
- [2] Martin Arjovsky, Soumith Chintala, and Léon Bottou. Wasserstein gan. *arXiv preprint arXiv:1701.07875*, 2017.
- [3] Frédéric Bastien, Pascal Lamblin, Razvan Pascanu, James Bergstra, Ian Goodfellow, Arnaud Bergeron, Nicolas Bouchard, David Warde-Farley, and Yoshua Bengio. Theano: new features and speed improvements. *arXiv preprint arXiv:1211.5590*, 2012.
- [4] David Berthelot, Tom Schumm, and Luke Metz. Began: Boundary equilibrium generative adversarial networks. *arXiv preprint arXiv:1703.10717*, 2017.
- [5] Miguel A. Carreira-Perpinan. Mode-finding for mixtures of gaussian distributions. *IEEE Transactions on Pattern Analysis and Machine Intelligence*, 22(11):1318–1323, 2000.
- [6] Miguel Á Carreira-Perpiñán and Christopher KI Williams. On the number of modes of a gaussian mixture. In *International Conference on Scale-Space Theories in Computer Vision*, pages 625–640. Springer, 2003.
- [7] Sander Dieleman, Jan Schlüter, Colin Raffel, Eben Olson, Søren Kaae Sønderby, Daniel Nouri, Daniel Maturana, Martin Thoma, Eric Battenberg, Jack Kelly, Jeffrey De Fauw, Michael Heilman, Diogo Moitinho de Almeida, Brian McFee, Hendrik Weideman, Gábor Takács, Peter de Rivaz, Jon Crall, Gregory Sanders, Kashif Rasul, Cong Liu, Geoffrey French, and Jonas Degraeve. Lasagne: First release., 2015.
- [8] Vincent Dumoulin, Ishmael Belghazi, Ben Poole, Alex Lamb, Martin Arjovsky, Olivier Mastropietro, and Aaron Courville. Adversarially learned inference. *arXiv preprint arXiv:1606.00704*, 2016.
- [9] Ishan Durugkar, Ian Gemp, and Sridhar Mahadevan. Generative multi-adversarial networks. *arXiv preprint arXiv:1611.01673*, 2016.

- [10] William Fedus, Mihaela Rosca, Balaji Lakshminarayanan, Andrew M Dai, Shakir Mohamed, and Ian Goodfellow. Many paths to equilibrium: Gans do not need to decrease adivergence at every step. *arXiv preprint arXiv:1710.08446*, 2017.
- [11] Ian Goodfellow. Nips 2016 tutorial: Generative adversarial networks. *arXiv preprint arXiv:1701.00160*, 2016.
- [12] Ian Goodfellow, Jean Pouget-Abadie, Mehdi Mirza, Bing Xu, David Warde-Farley, Sherjil Ozair, Aaron Courville, and Yoshua Bengio. Generative adversarial nets. In *Advances in neural information processing systems*, pages 2672–2680, 2014.
- [13] Ishaan Gulrajani, Faruk Ahmed, Martin Arjovsky, Vincent Dumoulin, and Aaron Courville. Improved training of wasserstein gans. *arXiv preprint arXiv:1704.00028*, 2017.
- [14] Martin Heusel, Hubert Ramsauer, Thomas Unterthiner, Bernhard Nessler, and Sepp Hochreiter. Gans trained by a two time-scale update rule converge to a local nash equilibrium. In *Advances in Neural Information Processing Systems*, pages 6629–6640, 2017.
- [15] Diederik P Kingma and Max Welling. Auto-encoding variational bayes. *arXiv preprint arXiv:1312.6114*, 2013.
- [16] Naveen Kodali, Jacob Abernethy, James Hays, and Zsolt Kira. On convergence and stability of gans. *arXiv preprint arXiv:1705.07215*, 2017.
- [17] Alex Krizhevsky and Geoffrey Hinton. Learning multiple layers of features from tiny images. 2009.
- [18] Alex Krizhevsky, Ilya Sutskever, and Geoffrey E Hinton. Imagenet classification with deep convolutional neural networks. In *Advances in neural information processing systems*, pages 1097–1105, 2012.
- [19] Yann LeCun. The mnist database of handwritten digits. <http://yann.lecun.com/exdb/mnist/>, 1998.
- [20] Jae Hyun Lim and Jong Chul Ye. Geometric GAN. 2017.
- [21] Ziwei Liu, Ping Luo, Xiaogang Wang, and Xiaoou Tang. Deep learning face attributes in the wild. In *Proceedings of International Conference on Computer Vision (ICCV)*, 2015.
- [22] Mario Lucic, Karol Kurach, Marcin Michalski, Sylvain Gelly, and Olivier Bousquet. Are gans created equal? a large-scale study. *arXiv preprint arXiv:1711.10337*, 2017.
- [23] Lars Mescheder, Sebastian Nowozin, and Andreas Geiger. The numerics of gans. *arXiv preprint arXiv:1705.10461*, 2017.
- [24] Luke Metz, Ben Poole, David Pfau, and Jascha Sohl-Dickstein. Unrolled generative adversarial networks. *arXiv preprint arXiv:1611.02163*, 2016.
- [25] G. K. Monatsh. Mehrdimensionale geometrie. *Monatshefte für Mathematik und Physik*, 1907.
- [26] Yunus Saatchi and Andrew Gordon Wilson. Bayesian GAN. In *Advances in Neural Information Processing Systems*, 2017.
- [27] Akash Srivastava, Lazar Valkoz, Chris Russell, Michael U Gutmann, and Charles Sutton. Veegan: Reducing mode collapse in gans using implicit variational learning. In *Advances in Neural Information Processing Systems*, pages 3310–3320, 2017.
- [28] Christian Szegedy, Wei Liu, Yangqing Jia, Pierre Sermanet, Scott Reed, Dragomir Anguelov, Dumitru Erhan, Vincent Vanhoucke, and Andrew Rabinovich. Going deeper with convolutions. In *Proceedings of the IEEE conference on computer vision and pattern recognition*, pages 1–9, 2015.
- [29] Thomas Unterthiner, Bernhard Nessler, Günter Klambauer, Martin Heusel, Hubert Ramsauer, and Sepp Hochreiter. Coulomb gans: Provably optimal nash equilibria via potential fields. *arXiv preprint arXiv:1708.08819*, 2017.
- [30] Tom White. Sampling generative networks. *arXiv preprint arXiv:1609.04468*, 2016.
- [31] Svante Wold, Kim Esbensen, and Paul Geladi. Principal component analysis. *Chemometrics and intelligent laboratory systems*, 2(1-3):37–52, 1987.
- [32] Han Xiao, Kashif Rasul, and Roland Vollgraf. Fashion-mnist: a novel image dataset for benchmarking machine learning algorithms. *arXiv preprint arXiv:1708.07747*, 2017.

- [33] Junbo Zhao, Michael Mathieu, and Yann LeCun. Energy-based generative adversarial network. *arXiv preprint arXiv:1609.03126*, 2016.